ELSEVIER

Coordination Chemistry Reviews 233–234 (2002) 207–222

COORDINATION CHEMISTRY REVIEWS

www.elsevier.com/locate/ccr

Chains, planes, and antimonides

Allison M. Mills, Robert Lam, Michael J. Ferguson, Laura Deakin, Arthur Mar *

Department of Chemistry, University of Alberta, Edmonton, AB, Canada T6G 2G2

Received 19 September 2001; accepted 8 March 2002

Contents

Abstract

Ternary rare-earth main-group pnictides $RE_xM_yPn_z$ where M is a Group 13 or 14 element and Pn is P, As, Sb, or Bi form an emerging class of solid state compounds that frequently display extensive homoatomic M–M and Pn–Pn bonding in addition to heteroatomic M–Pn bonding in their anionic substructures. Their structures, properties, and bonding are discussed, with a focus on the antimonides, which have been most heavily investigated.

Keywords: Pnictides; Antimonides; Rare-earth; Structural chemistry

1. Introduction

Extended solid-state compounds fall between two extremes: intermetallics such as Cu_5Zn_8 in which the electronegativity difference between components is small and structures are controlled by the valence electron concentration, and classical ionic compounds such as NaCl in which the electronegativity difference is large and full electron transfer is assumed to take place so that atoms conform to the octet rule [1–3]. In both extremes,

Abbreviations: A, alkali or alkaline-earth metal; RE, rare-earth metal; M, main-group element (Group 13 or 14); Pn, pnicogen (P, As, Sb, Bi); CN, coordination number; EDX, energy-dispersive X-ray; T_C, transition temperature for a superconductor or Curie temperature for a ferromagnet; T_N, Néel temperature; H_C, critical field; μ_B, Bohr magneton; M_{sat}, saturation magnetization; $^1_\infty$, one-dimensional chain; $^2_\infty$, two-dimensional layer; $_\infty{}^3$, three-dimensional network.

* Corresponding author. Tel.: +1-780-492-5592; fax: +1-780-492-8231.

E-mail address: arthur.mar@ualberta.ca (A. Mar).

0010-8545/02/$ - see front matter © 2002 Elsevier Science B.V. All rights reserved.
PII: S0010-8545(02)00097-8

bonding is nondirectional and atoms pack as efficiently as possible to attain dense arrangements or maximized electrostatic attractions. For the vast majority of combinations of elements, however, the electronegativity differences are intermediate and the resulting structures display a bewildering variety of bonding patterns. The question that arises is how one accounts for the bonding in these compounds. It is natural for chemists to gravitate towards the octet rule and assume, even though bonding is clearly no longer ionic in these compounds, that the more electropositive component transfers its valence electrons entirely to the more electronegative component, which may still need to form additional homoatomic bonds to achieve a closed-shell configuration. Known as the Zintl concept, this application of the octet rule to 'ionic compounds of reduced polarity', as it were, seems so obvious as to be trivial, but when these compounds are viewed from the other extreme as 'polar intermetallics', as they are normally called, it is remarkable that the rule should work as well as it does [4–6].

Most Zintl compounds studied in the past have involved combinations of alkali or alkaline-earth metals with the p-block elements. As the electronegativity differences are reduced by choosing the p-block element further to the left (e.g. $CaAl_4$ [7]) or down (e.g. $Ca_{31}Sn_{20}$ [8]) in the periodic table, the ionic picture becomes less realistic and the Zintl concept must be reformulated in terms of filled bonding (or nonbonding) states and unfilled antibonding states to account for the clusters and networks that now abound in the anionic substructures. New and unusual modes of bonding might also be found by use of a less electropositive component. This could be done by selecting an element further to the top of the periodic table; thus, in binary lithium silicides and germanides, it is believed that Li orbitals are substantially involved in covalent bonding to the p-element frameworks [9]. Alternatively, an element further to the right of the periodic table, viz. the rare earths (RE), could be chosen. Binary compounds of RE and p-block elements such as $SmSb_2$ [10] or La_3In_5 [11] featuring multicentre bonding can be understood in terms of the modernized reformulation of the Zintl concept. Our point of departure begins here.

Six years ago, we set out to investigate the ternary systems RE–M–Pn, where M is a Group 13 or 14 element and Pn is a pnicogen (P, As, Sb, Bi), focusing primarily on the antimonides. The extensive work of Eisenmann, Cordier, and Schäfer had revealed a phenomenally rich chemistry in the corresponding ternary alkali and alkaline-earth main-group pnictides A–M–Pn [12]. For the most part, the structures of these latter compounds contain trigonal planar or tetrahedral units, centred by the less electronegative M atom, that may be condensed into extended heteroatomic anionic substructures consisting of normal $2c–2e^-$ bonds. As could be anticipated by inspection of the structures of binary rare-earth pnictides, new bonding patterns emerge on going to the ternary rare-earth main-group pnictides. 'Nonclassical' bonding involving fractional bond orders recurs in ternary rare-earth main-group antimonides. The hypervalent bonding patterns that are adopted by heavier late p-block elements such as Sb and Te have been reviewed by Papoian and Hoffmann, who assert the use of a refined electron counting scheme to extend the Zintl concept to these compounds [13,14]. Hypervalent bonding in antimonides had, of course, been implicated earlier [9]. As structural chemists, we were interested in how the anionic substructure would partition the electrons available to it to form homo- and heteroatomic bonds for these compounds at the Zintl border, and what sort of systematizing principles would be apparent to organize their structures. A recent review on early-transition-metal-rich antimonides [15] complements the present one, illustrating that these nonclassical anionic networks persist even in intermetallic antimonides of more greatly reduced electronegativity differences, as occurs, for instance, in $(Zr, V)_{13}Sb_{10}$ [16].

This review summarizes the syntheses, structures, bonding, and properties of ternary (and some quaternary) rare-earth main-group pnictides $RE_xM_yPn_z$. The main-group element M has been restricted to Group 13 or 14 to ensure that we are dealing with anionic Pn (i.e. pnictides as opposed to chalcopnictates or halopnictates). Nitrides are not considered because of their very different chemistry. Most of the compounds described are antimonides, but a smaller number of phosphides, arsenides, and bismuthides have also been identified.

Table 1
Rare-earth main-group phosphides and arsenides

Compound	Structure type	Reference
$RESiP_3$ (RE = La, Ce, Pr)	$LaSiAs_3$-type (*Pbca*)	[17–21]
$LaSiAs_3$	$LaSiAs_3$-type (*Pbca*)	[22–24]
$RESiP_3$ (RE = Ce, Pr, Nd, Sm)	$CeSiP_3$-type ($Pn2_1a$)	[17–21]
$RESiAs_3$ (RE = La, Ce, Pr)	$CeSiP_3$-type ($Pn2_1a$)	[22–24]
$LaSiP_3$	'X-type' (unknown structure)	[20]
$RESiP_3$ (RE = Ce, Pr)	'C-type' (unknown structure)	[20]
$RESi_2P_6$ (RE = La, Ce, Pr, Nd)	$LaSi_2P_6$-type ($Cmc2_1$)	[26]
La_5M_3P (M = Ge, Pb)	Stuffed Mn_5Si_3-type ($P6_3/mcm$)	[27,28]
La_5M_3As (M = Ge, Pb)	Stuffed Mn_5Si_3-type ($P6_3/mcm$)	[27,28]
$Eu_{14}AlP_{11}$	$Ca_{14}AlSb_{11}$-type ($I4_1/acd$)	[29]
$Eu_6Ga_2P_6$	$Ba_6Al_2Sb_6$-type (*Cmca*)	[29]
$Na_3(Na_xEu_{3-x})MP_4$ (M = Si, Ge, Sn, Pb)	Na_6ZnO_4-type ($P6_3mc$)	[31,32]
$Na_3(Na_xEu_{3-x})MAs_4$ (M = Si, Ge, Sn, Pb)	Na_6ZnO_4-type ($P6_3mc$)	[31,32]

2. Rare-earth main-group pnictides

2.1. Phosphides and arsenides

There are surprisingly few rare-earth main-group phosphides and even fewer arsenides, as listed in Table 1.

The most well-studied are the rare-earth silicon phosphides and arsenides. These phases were first identified as byproducts of reactions in silica tubes, which were attacked above 900 °C [17,18]. Several types of phases are formed depending on the temperature and the pnicogen vapour pressure. Plate-shaped crystals $RESiP_3$ (RE = La–Nd, Sm) [19–21] and $RESiAs_3$ (RE = La–Pr) [22–24] exist in at least two well-characterized structure types that were originally called 'F-type' with the assumption of an F-centred orthorhombic cell and 'P-type' with the assumption of a primitive orthorhombic cell. In fact, the F-type phase, whose structure was first determined for $LaSiAs_3$, was shown to adopt a primitive cell (*Pbca*) [22]. To avoid confusion, we refer to these two phases as the $LaSiAs_3$-type (*Pbca*) and the $CeSiP_3$-type ($Pn2_1a$). Fig. 1 shows their structures, which are closely related and have unit cells with $a \approx 6$, $b \approx 6$, and $c \approx 25$ Å. Both structures consist of layers of composition $[SiPn_2]^{2-}$ and $[Pn]^{1-}$ stacked along the *c* axis and separated by the RE^{3+} cations. The $[SiPn_2]$ layers are built up of corner-sharing $SiPn_4$ tetrahedra, creating six-membered rings in a boat conformation. In the structure of $CeSiP_3$, the [Pn] layers contain segregated *cis–trans* chains of pnicogen atoms running along the *b* direction; the P–P distances are 2.249(7)–2.328(7) Å within the chains but more than 3.7 Å between the chains [21]. In the structure of $LaSiAs_3$, the [Pn] layers resemble much more closely an undistorted square sheet, with As–As distances of 2.99(2)–3.04(1) Å [23]. The As atoms have oblate-shaped thermal ellipsoids that are very large within the *ab*

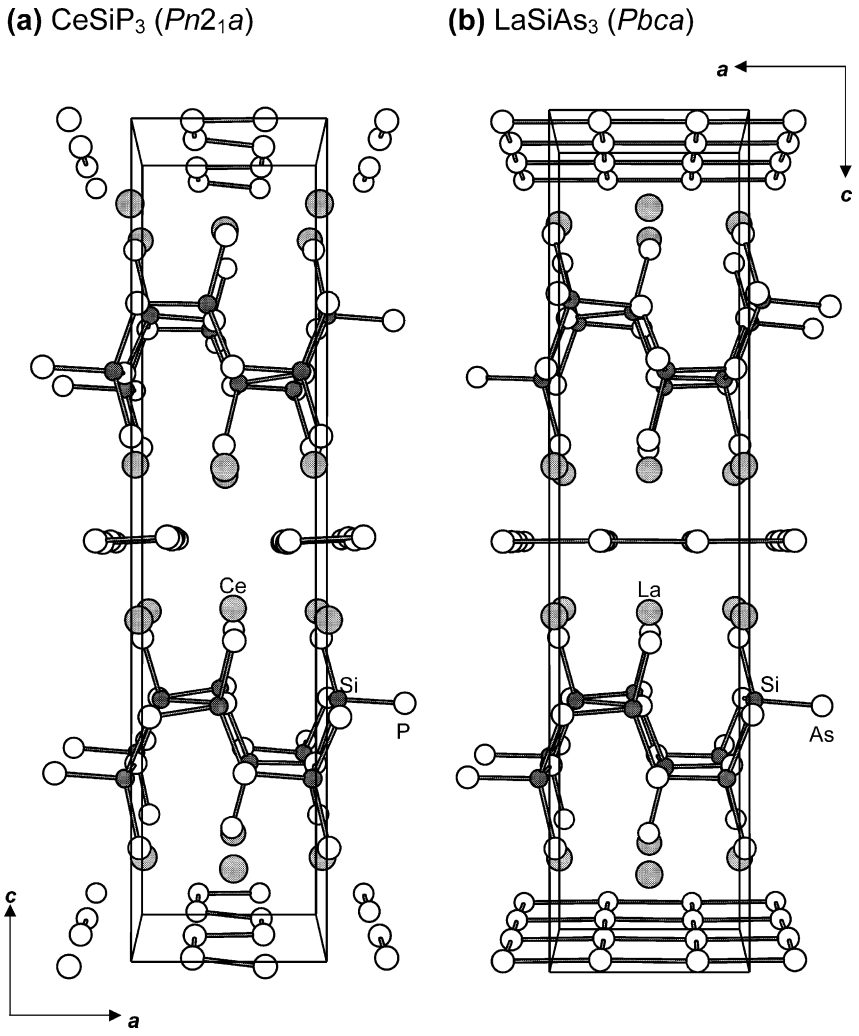

Fig. 1. Comparison of: (a) $CeSiP_3$- [21]; and (b) $LaSiAs_3$-type [23] structures, built up of layers of composition $[SiPn_2]$ and [Pn] separated by the RE atoms. Here and in all subsequent figures, the large shaded circles are RE atoms, the small solid circles are M (Group 13 or 14) atoms, and the medium open circles are Pn atoms.

plane, however, suggesting that the square net is prone to distortion. Indeed, $LaSiAs_3$ undergoes a phase transformation between the two structure types, with the high-temperature structure ($LaSiAs_3$-type) having the undistorted square sheet being formed at 900 °C and the low-temperature structure ($CeSiP_3$-type) having the distorted square sheet being formed at 780 °C [24]. A comparison of densities also implies that the $LaSiAs_3$-type is the low-pressure phase and the $CeSiP_3$-type is the high-pressure phase. The distortion of the square net is reminiscent of that seen in GdPS [25]. $LaSiAs_3$ thus provides a nice illustration of how a square $^{2}_{\infty}[As]^{1-}$ sheet, representing a hypervalent geometry for As in a two-dimensional arrangement, transforms through a Peierls distortion to a classical geometry of zigzag $^{1}_{\infty}[As]^{1-}$ chains with reduced dimensionality [13]; that is, four weak As–As bonds are electronically equivalent to two strong As–As bonds. The difference between the $CeSiP_3$- and $LaSiAs_3$-type structures does not merely involve a redistribution of electron density within the [Pn] sheets, however. The RE atoms are stacked differently in the two structures (they are positioned directly opposite to each other above and below the [Pn] sheet in $LaSiAs_3$ whereas they are staggered in $CeSiP_3$).

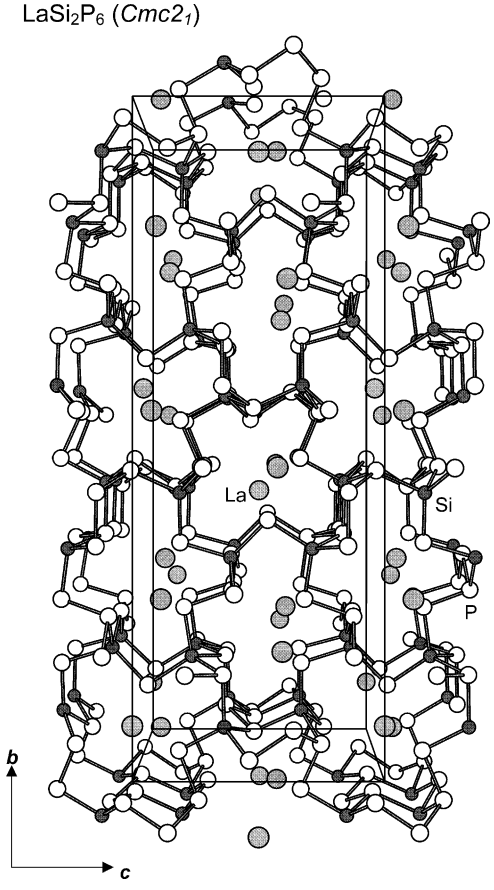

Fig. 2. Three-dimensional structure of $LaSi_2P_6$ [26] built up of corner-sharing SiP_4 tetrahedra in the anionic framework.

An 'X-type' phase of $LaSiP_3$ and 'C-type' phases of $CeSiP_3$ and $PrSiP_3$ were also reported, but their structures remain unknown [20].

Needle-shaped crystals $RESi_2P_6$ (RE = La–Nd) were produced by direct reaction of the elements at 900 °C or in the presence of a Sn flux at 800 °C [26]. Although it can be described as consisting of layers connected by P–P bridges, the anionic substructure of $RESi_2P_6$ is really three-dimensional in extent; it is built up of corner-sharing SiP_4 tetrahedra and forms channels within which the RE cations reside, as shown in Fig. 2. There are a number of P–P bonds within the anionic substructure, but all of them are normal 2c–2e$^-$ bonds (2.207 Å on average in $LaSi_2P_6$), so that the Zintl concept gives a satisfactory formulation for $RESi_2P_6$, or with $Z = 16$ within the unit cell, $RE_{16}Si_{32}P_{96}$: $(RE^{3+})_{16}(Si^{4+})_{32}(P^{3-})_{24}(P^{2-})_{40}(P^{1-})_{24}(P^{0})_8$ if oxidation states are considered.

Ternary interstitial derivatives La_5M_3P or La_5M_3As (M = Ge, Pb) are known in which P or As atoms are stuffed into the binary La_5Ge_3 and La_5Pb_3 host structures [27,28]. These were prepared by reactions in Ta tubes jacketed by silica, generally at temperatures above 1050 °C and with the use of binary LaP or LaAs. The compounds adopt the stuffed hexagonal Mn_5Si_3-type structure, a very common one, in which the interstitial P or As atoms reside in the centres of La_6 octahedra forming confacial chains along the *c* direction. Ge or Pb atoms bridge the edges of the shared faces of the La_6 octahedra and they also connect the confacial chains to parallel linear chains of La atoms. Unlike the parent La_5M_3 hosts which are metallic, the La_5M_3Pn compounds are valence-precise and show semiconducting behaviour. La_5Ge_3P, for instance, has an experimental band gap of ca. 0.11 eV and is diamagnetic [27].

The remaining entries in Table 1 involve Eu acting in its capacity in the divalent state as a pseudo-alkaline-earth metal. $Eu_{14}AlP_{11}$, obtained from reaction of EuP and Al in a Nb tube at 1100 °C [29], is isostructural to the well-known family $A_{14}MPn_{11}$ where typically A = Ca, Sr, Ba and M = Al, Ga, Mn [4]. In addition to discrete P^{3-} anions and AlP_4^{9-} tetrahedra, the structure of $Eu_{14}AlP_{11}$ contains a linear P_3^{7-} trimer containing hypervalent 3c–4e$^-$ bonding: $(Eu^{2+})_{14}(AlP_4^{9-})(P_3^{7-})-(P^{3-})_4$. Similarly, $Eu_6Ga_2P_6$, synthesized from Eu + EuP + GaP in a steel ampoule at 1100 °C, is isostructural to $Ba_6Ga_2P_6$ and consists of isolated pairs of edge-sharing GaP_4 tetrahedra: $(Eu^{2+})_6(Ga_2P_6^{12-})$ [30]. After $Na_3(Na_xEu_{3-x})SiAs_4$ was first discovered in a reaction of Na, Eu, and As in a silica tube [31], the family of quaternaries $Na_3(Na_xEu_{3-x})MP_4$ and $Na_3(Na_xEu_{3-x})MAs_4$ (M = Si, Ge, Sn, Pb) was elaborated by reaction of the elements in Nb tubes at 1000 °C [32]. Adopting the Na_6ZnO_4-type structure, they contain isolated MPn_4^{8-} tetrahedra. Charge balance then demands the formula $(Na^+)_3(Na_xEu_{3-x})^{5+}(MPn_4^{8-})$.

Table 2
Rare-earth main-group antimonides and bismuthides

Compound	Structure type	Reference
$La_{13}Ga_8Sb_{21}$	$La_{13}Ga_8Sb_{21}$-type (*P6/mmm*)	[34,35]
$RE_{12}Ga_4Sb_{23}$ (RE = La, Ce, Pr, Nd, Sm)	$Pr_{12}Ga_4Sb_{23}$-type (*Immm*)	[34,35]
$REGaSb_2$ (RE = La, Sm)	$SmGaSb_2$-type ($C222_1$)	[36]
$REGaSb_2$ (RE = Ce, Pr, Nd)	$NdGaSb_2$-type ($I4_1/amd$)	[36]
$Sm_xGa_{1-x}Sb$	Zincblende-type ($F\bar{4}3m$)	[37]
$SmGaSb_2$	NaCl-type ($Fm\bar{3}m$)	[37]
$REIn_{0.8}Sb_2$ (RE = La, Ce, Pr, Nd)	$LaIn_{0.8}Sb_2$-type ($P2_1/m$)	[40]
$Yb_5In_2Sb_6$	$Ba_5Al_2Bi_6$-type (*Pbam*)	[41]
$Eu_{14}InSb_{11}$	$Ca_{14}AlSb_{11}$-type ($I4_1/acd$)	[48]
Ce_2GeSb_3	$ThGe_2$-type (*Cmmm*)	[49]
Ce_3GeSb	La_3GeIn-type?	[49]
$Ce_5Ge_3Sb_2$	Unknown structure	[49]
La_5M_3Sb (M = Ge, Pb)	Stuffed Mn_5Si_3-type ($P6_3/mcm$)	[27]
$RE_6Ge_{5-x}Sb_{11+x}$ (RE = La, Ce, Pr, Nd, Sm, Gd, Tb, Dy)	$RE_6Ge_{5-x}Sb_{11+x}$-type (*Immm*)	[51,52]
La_4MSb_2 (M = Sn, Pb)	*anti*-Th_3P_4-type ($I\bar{4}3d$)	[53]
$RESn_xSb_2$ (RE = La, Ce, Pr, Nd, Sm)	$LaSn_xSb_2$-type (*Cmcm*)	[55,56]
$EuSn_3Sb_4$	$EuSn_3Sb_4$-type (*Pnma*)	[57]
$REGa_xSn_ySb_2$	Disordered RE-$GaSb_2$–$RESn_xSb_2$	[60]
$REIn_xSn_ySb_2$	Disordered $REIn_{0.8}$-Sb_2–$RESn_xSb_2$?	[61]
$Eu_{14}InBi_{11}$	$Ca_{14}AlSb_{11}$-type ($I4_1/acd$)	[48]
La_4SnBi_2	*anti*-Th_3P_4-type ($I\bar{4}3d$)	[53]
$La_4Pb_xBi_{3-x}$	*anti*-Th_3P_4-type ($I\bar{4}3d$)	[53]
$LaGaBi_2$?	Unknown structure (hexagonal)	[62]

Although the five positive charges could be distributed over the disordered Na/Eu site as $(Na^+)(Eu^{2+})_2$, the refined occupancy is somewhat less than 2/3 Eu in all cases, suggesting that a small amount of trivalent Eu^{3+} is present.

2.2. Antimonides

A growing number of rare-earth main-group antimonides is being revealed, as listed in Table 2.

2.2.1. RE–Al–Sb

Investigation of part of the Ce–Al–Sb phase diagram by arc-melting and annealing samples at 500 °C for 150 h revealed no ternary compounds [33], although the Sb-rich (> 50% Sb) region deserves examination, as do other RE–Al–Sb systems.

2.2.2. RE–Ga–Sb

At least four structure types have been well characterized in the RE–Ga–Sb system: $La_{13}Ga_8Sb_{21}$-[34,35], $Pr_{12}Ga_4Sb_{23}$- [34,35], $SmGaSb_2$- [36], and $NdGaSb_2$-types [36]. (There is also a cursory study of the pseudobinary SmSb–GaSb phase diagram that suggests the existence of a limited solid solution for $Sm_xGa_{1-x}Sb_2$ $(0 < x < 0.1)$ with GaSb as the end member and a ternary $SmGaSb_2$ compound with the NaCl-type structure [37].) The synthetic conditions for preparing these phases have not yet been optimized. A mixture of La + 2 Ga + 2 Sb heated at 900 °C for 3 days, cooled to 500 °C in 4 days, and cooled to room temperature in 12 h produced needle-shaped crystals of $La_{13}Ga_8Sb_{21}$ and plate-shaped crystals of $LaGaSb_2$ ($SmGaSb_2$-type). For RE = Ce–Nd, analogous reactions produced plate-shaped crystals of $REGaSb_2$ as well as unreacted Ga, which apparently serves as a flux when present in excess. $REGaSb_2$ (RE = La–Nd, Sm) can be obtained by stoichiometric reaction of the elements (RE + Ga + 2 Sb), but the product is generally contaminated by $RE_{12}Ga_4Sb_{23}$ phases. However, $RE_{12}Ga_4Sb_{23}$ (RE = La–Nd, Sm) can be produced in relatively pure form through stoichiometric reactions 12 RE + 4 Ga + 23 Sb. These observations point to complex behaviour in these phase systems. Woe betides the

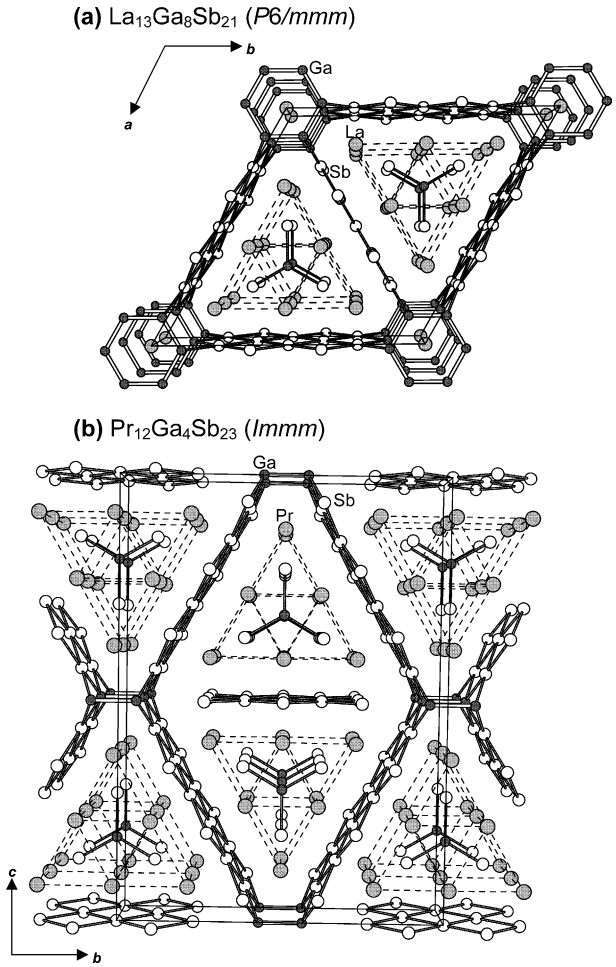

Fig. 3. Comparison of the structures of: (a) $La_{13}Ga_8Sb_{21}$; and (b) $Pr_{12}Ga_4Sb_{23}$ [34]. The dashed lines outline the assemblies of RE_6 trigonal prisms common to both structures.

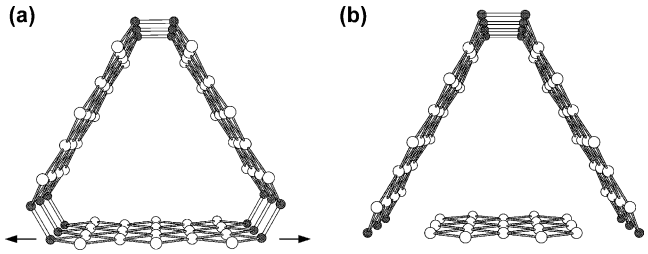

Fig. 4. Comparison of the 21-atom channels in: (a) $La_{13}Ga_8Sb_{21}$, composed of five-atom-wide Sb ribbons; and (b) $Pr_{12}Ga_4Sb_{23}$, composed of two six-atom-wide Sb ribbons and one five-atom-wide Sb ribbon [34]. The Sb ribbons are linked by Ga atoms.

experimentalist who fails to take precautions to distinguish between the similar appearance of these crystals.

$La_{13}Ga_8Sb_{21}$ and $RE_{12}Ga_4Sb_{23}$ tend to be needle-shaped and have crystal structures, shown in Fig. 3, that are characterized by channels outlined by 21-membered rings [34]. In the $La_{13}Ga_8Sb_{21}$-type structure (Fig. 3a), these channels are made up of five-atom-wide ribbons of Sb atoms connected by Ga–Ga bonds. In turn, these Ga–Ga bonds form a puckered six-membered Ga_6-ring, assumed to be in a chair conformation, around the origin of the unit cell. In the $Pr_{12}Ga_4Sb_{23}$-type structure (Fig. 3b), these channels are made up of isolated five-atom-wide Sb ribbons, and six-atom-wide Sb ribbons connected by Ga–Ga bonds forming Ga_2-pairs. The loss of equivalence of the three Ga/Sb segments outlining these channels on going from $La_{13}Ga_8Sb_{21}$ to $Pr_{12}Ga_4Sb_{23}$ is accompanied by a lowering of the crystallographic symmetry from hexagonal to orthorhombic (Fig. 4). Within the channels in both structures, there are trigonal planar $GaSb_3$ units. Each of the Ga and Sb atoms making up the $GaSb_3$ trigonal planes is coordinated by six RE atoms in a trigonal prism. These trigonal prismatic columnar assemblies then extend along the needle-axis direction. $La_{13}Ga_8Sb_{21}$ features an unusual coordination for the La atom at the origin of the unit cell, being sandwiched by two puckered Ga_6-rings. It is noteworthy that the $La_{13}Ga_8Sb_{21}$ structure forms uniquely for RE = La, even though the $La_{13}Ga_8Sb_{21}$ and $Pr_{12}Ga_4Sb_{23}$ structure types are closely related. Although this CN12 geometry is atypical, it is observed for other RE in, for example, Gd_5CuGa_9 ($CeCd_2$-type) [38] or $YbGa_2$ ($CaIn_2$-type) [39]. The unique occurrence of $La_{13}Ga_8Sb_{21}$ may be related to the presence of the rather short Ga–Ga bond (2.422(5) Å) within the Ga_6-rings compared to the more normal Ga–Ga bond (2.586(4) Å) of the Ga_2-pair in $Pr_{12}Ga_4Sb_{23}$. Substitution of a smaller RE for La in $La_{13}Ga_8Sb_{21}$ would contract the structure to an extent that the Ga–Ga bonds linking the Sb ribbons would become unreasonably short.

The $SmGaSb_2$- and $NdGaSb_2$-type structures are layered [36], as shown in Fig. 5; correspondingly, crystals tend to be plate-shaped. They are stacking

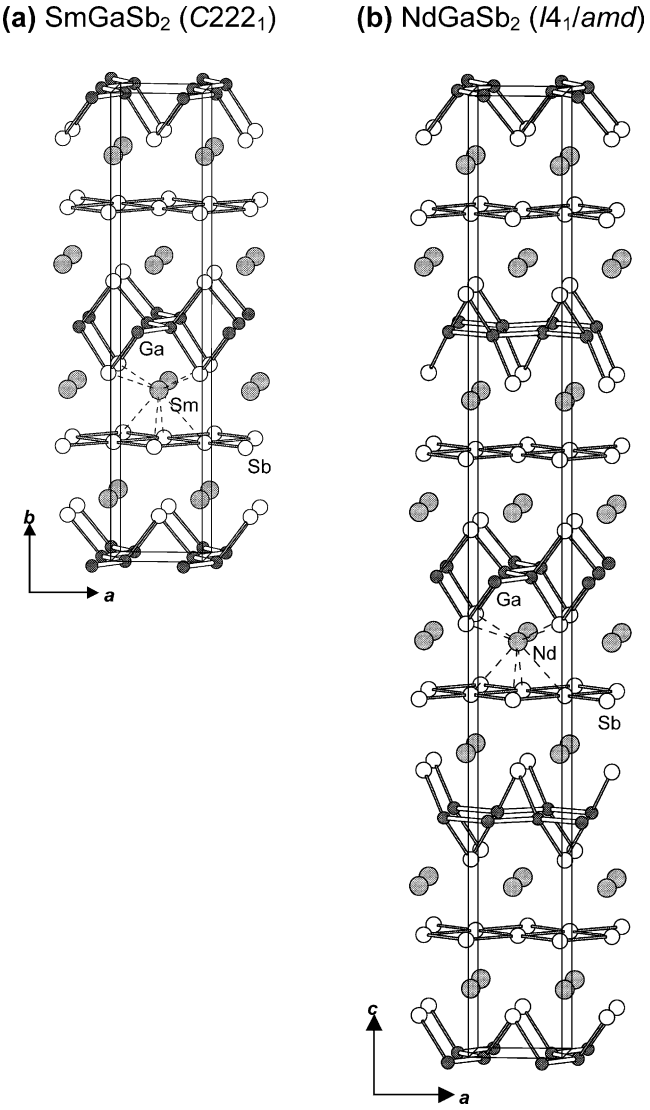

Fig. 5. Comparison of the layered: (a) $SmGaSb_2$- and (b) $NdGaSb_2$-type structures [37]. The coordination around a RE atom by Sb atoms is shown in each structure.

variants of each other and contain $^2_\infty$[GaSb] and $^2_\infty$[Sb] layers separated by the RE cations. The Ga atoms in the $^2_\infty$[GaSb] layers are coordinated in a tetrahedral fashion, $Ga(Ga_2Sb_2)$, such that the Ga atoms that serve as the ligands in one tetrahedron can be regarded as centres of adjacent tetrahedra, thereby forming infinite one-dimensional zigzag Ga chains containing Ga–Ga bonds of 2.539(2) Å in $SmGaSb_2$ and 2.605(3) Å in $NdGaSb_2$. In orthorhombic $SmGaSb_2$ ($C222_1$), these Ga chains run along the c axis and impart chirality to the structure. In tetragonal $NdGaSb_2$ ($I4_1/amd$), there is disorder of the Ga chains associated with a 50% occupancy of the Ga sites. All of the Ga chains in $SmGaSb_2$ are parallel and run along the c direction, whereas they are mutually perpendicular and run alternately along the a or b direction in $NdGaSb_2$. Why the $SmGaSb_2$-type structure forms for RE = La

and Sm whereas the $NdGaSb_2$-type structure forms for RE = Ce, Pr, Nd is unclear. It does not seem that there would be much energetic difference between one stacking variant and the other, and it may well be that adjustment of synthetic conditions could yield alternative polytypes. The $^2_\infty$[Sb] square nets are a common theme in structures of many antimonides. The Sb–Sb distances within these nonclassical square nets (3.0–3.1 Å) is suggestive of weak hypervalent bonding, which will be discussed in further detail later.

$La_{13}Ga_8Sb_{21}$ is found to be superconducting below $T_C = 2.4$ K [35]. All $RE_{12}Ga_4Sb_{23}$ compounds (RE = La, Ce, Pr, Nd, Sm) show metallic behaviour down to 2 K and have room temperature resistivities of about $1–2 \times 10^{-4}$ Ω cm, except for the Sm member which is about two orders of magnitude more resistive. It is surprising that $La_{13}Ga_8Sb_{21}$ is superconducting whereas $La_{12}Ga_4Sb_{23}$ is not, given the similarity of their crystal and electronic structures, but the manifestation of superconductivity can be quite sensitive to the precise shape of the Fermi surface. The properties of the $REGaSb_2$ series remain to be measured, but one would anticipate highly anisotropic behaviour given the layered nature of the structure.

2.2.3. *RE–In–Sb*

The reaction RE + In + 2 Sb at 570 °C for 1 day and 950 °C for 2 days, followed by cooling to 500 °C over 1 day and to room temperature over 5 h, produces ternary compounds that are substoichiometric in In, with an approximate formula $REIn_{0.8}Sb_2$ for RE = La, Ce, Pr, Nd [40]. The plate-shaped crystals of $REIn_{0.8}Sb_2$ are very soft and pliable making crystallographic studies somewhat of a challenge. $LaIn_{0.8}Sb_2$ is monoclinic ($P2_1/m$) and has a layered structure similar to that of $REGaSb_2$, with $_\infty{}^2$[$In_{0.8}$Sb] and $^2_\infty$[Sb] layers separated by the La cations, as shown in Fig. 6. Similar to the Ga chains in $REGaSb_2$, there are zigzag In chains in $LaIn_{0.8}Sb_2$. The larger size of In compared to Ga atoms as they are inserted between sandwiching Sb sheets imparts some differences. Within the zigzag chains, the In–In bond (2.967(5) Å) in $LaIn_{0.8}Sb_2$ is considerably longer than the Ga–Ga bond (ca. 2.5 Å) in either $REGaSb_2$ polytype. Whereas parallel Ga chains are coplanar in $REGaSb_2$, parallel In chains are slightly canted with respect to the planes of the surrounding Sb sheets in $LaIn_{0.8}Sb_2$. Moreover, the In atoms are now coordinated in a distorted square pyramidal fashion, $In(In_2Sb_3)$, in $LaIn_{0.8}Sb_2$, compared to the tetrahedral coordination of Ga in $REGaSb_2$. The substoichiometry of In (80% occupancy) can be interpreted on a local level by vacating every fifth site, on average, within the zigzag chains. Band structure calculations suggest that the substoichiometry occurs to avoid occupation of too many In–In antibonding states. The distance between neighbouring In zigzag chains is only 3.346(6) Å, but examination of the COOP curves in an extended Hückel calculation suggests that this interaction is insignificant compared to the intrachain distance.

$Yb_5In_2Sb_6$, prepared from reaction of a stoichiometric mixture of the elements at 700 °C [41], is a rare-earth

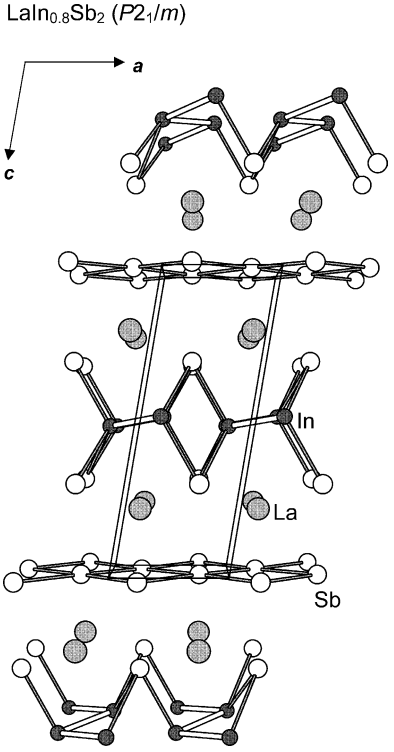

Fig. 6. The layered structure of $LaIn_{0.8}Sb_2$, with the zigzag In chains and square Sb nets shown [40].

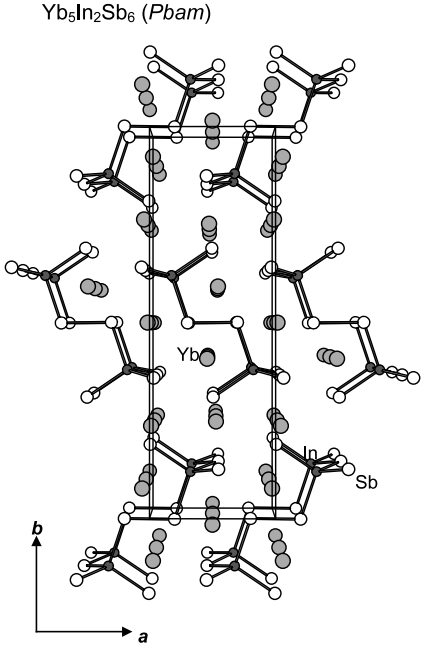

Fig. 7. Structure of $Yb_5In_2Sb_6$, built up of double chains of corner-sharing $InSb_4$ tetrahedra bridged through Sb_2-pairs [41].

analogue of the $A_5M_2Pn_6$ (A = Ca, Sr, Ba; M = Al, Ga, In; Pn = As, Sb, Bi) family. There are at least three structure types formed by members of this family. They are named inconsistently in the literature, so these are enumerated explicitly: (i) $Ca_5Ga_2As_6$ [42,43], $Ca_5Al_2Sb_6$ [44], $Ca_5Ga_2Sb_6$ [45], $Ca_5In_2Sb_6$ [45], $Sr_5In_2Sb_6$ [45], $Ba_5In_2Sb_6$ [46] (*Pbam*); (ii) $Ca_5Al_2Bi_6$ (*Pbam* but with a long ca. 23 Å axis) [47]; (iii) $Sr_5Al_2Sb_6$ (*Pnma*) [46]. $Yb_5In_2Sb_6$ is isostructural to $Ca_5Al_2Bi_6$ (after a unit cell transformation involving exchange of the *a* and *b* axes and an origin shift is applied). In $Yb_5In_2Sb_6$, two chains of corner-sharing $InSb_4$ tetrahedra are bridged together by Sb_2-pairs to form a $^1_\infty[In_2Sb_6]^{10-}$ double chain (Fig. 7). An interesting observation is that even though Yb^{2+} and Ca^{2+} have similar ionic radii, $Yb_5In_2Sb_6$ is not isostructural to $Ca_5In_2Sb_6$, whose structure involves a slightly different packing of the $^1_\infty[In_2Sb_6]^{10-}$ double chains. Moreover, the Sb–Sb distance within the Sb_2-pair is significantly longer in $Yb_5In_2Sb_6$ (2.944(2) Å) than in $Ca_5In_2Sb_6$ (2.863 Å). As alluded to earlier, the increased covalent character imparted by the use of RE instead of alkali or alkaline earth elements has important effects. To a first approximation, the Zintl formulation $(Yb^{2+})_5[(In^{3+})_2(Sb_2^{4-})(Sb^{3-})_4]$ appears satisfactory, but it belies the existence of the mixing of Yb and Sb states as confirmed by band structure calculations. Consequently, the band gap can be narrowed relative to that in an alkaline-earth analogue ($Yb_5In_2Sb_6$ has an experimental band gap of 0.2–0.4 eV and appears to be a highly doped p-type narrow gap semiconductor).

$Eu_{14}InSb_{11}$ was prepared by stoichiometric reaction of the elements in a Ta tube at ca. 1000 °C [48] and adopts the $Ca_{14}AlSb_{11}$-type structure, discussed earlier in the context of $Eu_{14}AlP_{11}$. It is paramagnetic at high temperatures with a magnetic moment $\mu_{eff} = 30(1)\ \mu_B$ and displays a divergence between the zero-field- and field-cooled susceptibilities below 15 K.

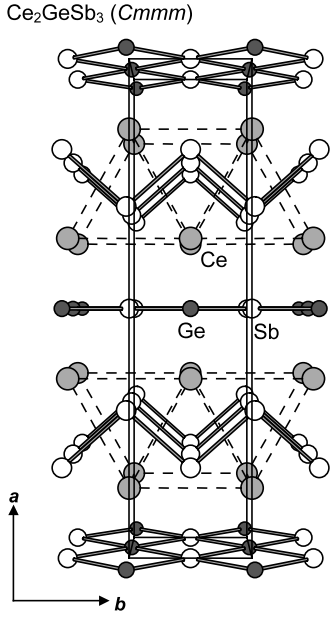

Fig. 8. Structure of Ce_2GeSb_3, an ordered ternary variant of the $ThGe_2$-type [49]. The dashed lines outline the RE_6 trigonal prisms.

2.2.4. *RE–Ge–Sb*

Investigation of the Ce–Ge–Sb phase diagram by arc-melting and annealing samples at 400 °C for 500 h revealed the ternary compounds Ce_2GeSb_3, Ce_3GeSb, and '$Ce_5Ge_3Sb_2$' [49]. Ce_2GeSb_3 is an ordered ternary variant of the $ThGe_2$-type structure (Fig. 8) [2]. The Ce atoms form trigonal prisms that are arranged in CrB-type slabs. The trigonal prisms are centred by Sb atoms so as to form zigzag chains containing Sb–Sb bonds of 3.111 Å. These slabs are separated by $^2_\infty$[GeSb] square sheets containing long Ge–Sb bonds of 3.166 Å. It is not clear how charges should be partitioned in the anionic framework. The zigzag chain is a classical geometry expected for Sb, but the Sb–Sb distance is a little too long for $2c–2e^-$ bonding. Likewise, the Ge–Sb distances in the $^2_\infty$[GeSb] square sheets are quite long. Ce_3GeSb is proposed to be isostructural to La_3GeIn [50]; although the cell parameters are reasonable, the atomic parameters reported for Ce_3GeSb are glaringly amiss. '$Ce_5Ge_3Sb_2$' represents the approximate composition of a phase with as yet undetermined structure.

The ternary interstitial derivative La_5Ge_3Sb is analogous to the corresponding phosphides and arsenides

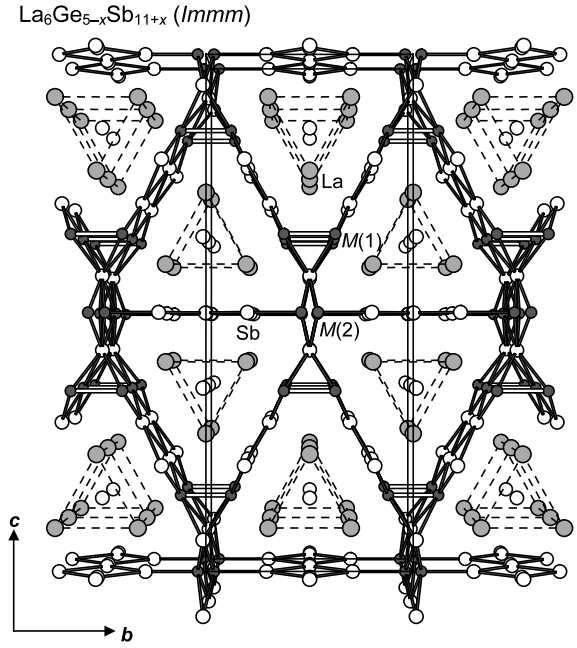

Fig. 9. Structure of $La_6Ge_{2.8(1)}Sb_{13.2(1)}$, built up of RE_6 trigonal prisms (outlined by dashed lines) within walls defined by Ge and Sb atoms [51]. M(1) and M(2) are disordered sites containing a mixture of Ge and Sb atoms.

discussed earlier, adopting the stuffed Mn_5Si_3-type structure [27].

The series $RE_6Ge_{5-x}Sb_{11+x}$ can be prepared for RE = La–Nd, Sm, Gd–Dy by stoichiometric reaction of the elements at 950 °C for 2 days, which gives needle-shaped crystals [51]. Partial disorder of the Ge and Sb atoms is responsible for the variable stoichiometry, which follows a trend of increasing Ge and decreasing Sb content as the size of the RE decreases. EDX analyses and single-crystal structure refinements give the composition of three representative members of this series as $La_6Ge_{2.8(1)}Sb_{13.2(1)}$, $Nd_6Ge_{3.6(1)}Sb_{12.4(1)}$, and $Gd_6Ge_{4.3(1)}Sb_{11.7(1)}$. Fig. 9 shows the structure of $La_6Ge_{2.8(1)}Sb_{13.2(1)}$, a relatively complex one displaying an interesting variety of anionic networks. It resembles the $Pr_{12}Ga_4Sb_{23}$-type structure in consisting of channels outlined by the metalloid atoms within which lie trigonal prisms of the RE atoms. The metalloid part of $RE_6Ge_{5-x}Sb_{11+x}$ can be deconstructed into three constituents: isolated Sb atoms within the centres of the RE trigonal prisms, three-atom-wide Sb ribbons, and kinked sheets folded at every fifth atom. Sites M(1) and M(2) contain a mixture of Ge and Sb atoms; further, M(2) can only be 50% occupied because of its proximity to a symmetry-equivalent position. The three-atom-wide Sb ribbons provide yet another example of the continuum of Sb strips of varying widths that can be excised from a square net. Although these strips are symmetrical with four equivalent Sb–Sb bonds of 3.0780(8) Å around each Sb centre in the case of $Gd_6Ge_{4.3(1)}Sb_{11.7(1)}$, they become distorted with two short (2.918(1) Å) and two long (3.333(1) Å) Sb–Sb bonds in the case of $La_6Ge_{2.8(1)}Sb_{13.2(1)}$, illustrating yet again how a hypervalent geometry for Sb can be converted to a classical geometry via a Peierls distortion. M(2) sites then border each side of the three-atom-wide Sb ribbons. Within the kinked sheets, some sites are exclusively occupied by Sb atoms, whereas M(1) contains Ge and Sb atoms. Substitution with a smaller RE contracts the $RE_6Ge_{5-x}Sb_{11+x}$ structure; the distances within these kinked sheets are then shortened so that they become more suitable for Ge–Ge instead of Ge–Sb bonds, accounting for the trend of increasing Ge and decreasing Sb content described above.

In $RE_6Ge_{5-x}Sb_{11+x}$, the arrangement of RE atoms in trigonal prismatic columns in which the intercolumn distances are significantly longer (>1 Å) than the intracolumn distances gives rise to the possibility of low-dimensional magnetic ordering. All members of the $RE_6Ge_{5-x}Sb_{11+x}$ series display metallic behaviour, but (except for the La member) they also show pronounced magnetic transitions indicative of interactions between conduction electrons and RE moments [52]. Table 3 summarizes the properties measured for $RE_6Ge_{5-x}Sb_{11+x}$. Long-range antiferromagnetic ordering ($T_N \leq 22$ K) occurs for RE = Ce, Pr, Nd, Sm, Gd, Tb. The Ce, Pr, and Nd members display metamagnetic behaviour at 2 K ($H_C = 1.0$–4.0 T) which is proposed to arise from a ferro- or ferrimagnetic spin arrangement within RE triangles, and an antiferromagnetic or canted spin arrangement between RE triangles of a column. The $Ce_6Ge_{5-x}Sb_{11+x}$ compound exhibits short-range one-dimensional magnetic interactions along RE columns as a result of uncompensated spins, manifested by an increase in the effective moment down to 5 K, below which long-range antiferromagnetic interactions between columns set in. $Gd_6Ge_{5-x}Sb_{11+x}$ is especially interesting as it undergoes a field-induced transition to a spin-flop phase, as evidenced from single-crystal magnetization and magnetoresistance experiments. The Tb and Dy members show minima in their resistivity curves that may also be a result of short-range interactions in this low-dimensional material.

Table 3
Electrical and magnetic properties of $RE_6Ge_{5-x}Sb_{11+x}$ [52]

Compound [a]	Properties
$La_6Ge_{2.8(1)}Sb_{13.2(1)}$	Metallic; nonmagnetic
$Ce_6Ge_{5-x}Sb_{11+x}$	Metallic; antiferromagnetic, $T_N = 4.0$ K; metamagnetic, $H_C = 1.0$ T at 2 K
$Pr_6Ge_{5-x}Sb_{11+x}$	Metallic; antiferromagnetic, $T_N = 2.7$ K; metamagnetic, $H_C = 1.5$ T at 2 K
$Nd_6Ge_{3.6(1)}Sb_{12.4(1)}$	Metallic; antiferromagnetic, $T_N = 4.2$ K; metamagnetic, $H_C = 4.0$ T at 2 K
$Sm_6Ge_{5-x}Sb_{11+x}$	Metallic; antiferromagnetic, $T_N = 8.3$ K
$Gd_6Ge_{4.3(1)}Sb_{11.7(1)}$	Metallic; antiferromagnetic, $T_N = 12.5$ K; spin-flopping, $H_{SF} = 1.85$ T, $H_C = 5.75$ T at 2 K
$Tb_6Ge_{5-x}Sb_{11+x}$	Metallic with resistivity minimum at 10 K; antiferromagnetic, $T_N = 22$ K; metamagnetic, $H_C > 7$ T at 2 K
$Dy_6Ge_{5-x}Sb_{11+x}$	Resistivity minimum at 150 K

[a] Compositions of the La, Nd, and Gd members were determined from structure refinements.

2.2.5. *RE–Sn–Sb*

The solid solution $La_4Sn_xSb_{3-x}$ (x = ca. 1.0) was prepared to study the effects of electron concentration on the superconducting transition of the parent La_4Sb_3, which adopts the cubic *anti*-Th_3P_4-type structure [53]. Whereas La_4Sb_3 superconducts below 0.25 K, La_4SnSb_2 shows no superconducting transition down to 0.08 K.

An early investigation of the '$LaSn_2$'–$LaSb_2$ section of the La–Sn–Sb phase diagram showed the existence of a ternary compound with tentative formula '$LaSnSb_2$' [54]. The structure was not determined at the time, but the X-ray powder diffraction pattern was provided. This phase has subsequently been shown to be part of a family of nonstoichiometric rare-earth tin antimonides $RESn_xSb_2$ with RE = La, Ce, Pr, Nd, Sm and ca. $0.1 \leq x \leq$ ca. 0.7 [55]. They can be prepared by reacting stoichiometric mixtures of the elements at 950 °C for

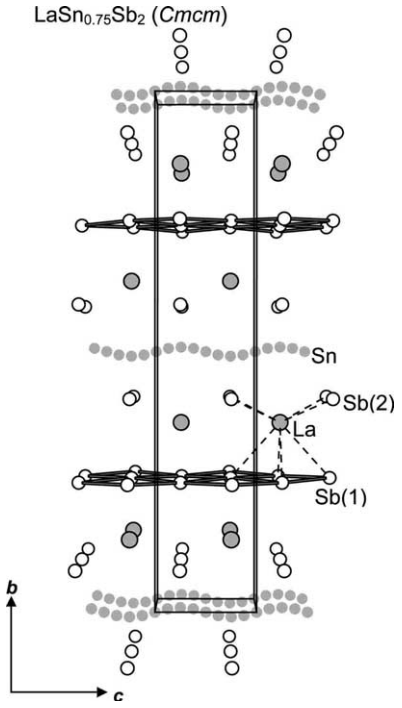

Fig. 10. Structure of $LaSn_{0.75}Sb_2$, built up by inserting chains of Sn sites between $RESb_2$ layers [55]. Each of the sites within these chains is only partially occupied with Sn atoms up to a maximum of 20%.

2 days, but they are also frequently found as byproducts when Sn is used as a flux in the synthesis of other ternary rare-earth antimonides! The orthorhombic structure of $LaSn_{0.75}Sb_2$ has been determined and it bears a resemblance to the other layered structures discussed earlier, $REGaSb_2$ and $REIn_{0.8}Sb_2$. Correspondingly, it is possible to describe the structure as consisting of $^2_\infty[Sn_{0.75}Sb]$ and $^2_\infty[Sb]$ layers separated by the La cations. However, the $RESn_xSb_2$ series is different from $REGaSb_2$ and $REIn_{0.8}Sb_2$ in that the Sn content is broadly variable. Fig. 10 shows an alternative way of describing the structure as consisting of chains of Sn sites inserted between $^2_\infty[RESb_2]$ layers. These chains contain three types of sites spaced at increments of ca. 0.6 Å that are occupied by Sn atoms. To arrive at reasonable Sn–Sn separations of ca. 2.8 Å, each of these sites can only be partially occupied to a maximum of about 20%, which corresponds to a limiting formula of '$LaSn_{0.8}Sb_2$', reasonably close to the crystallographically refined formula of $LaSn_{0.75(3)}Sb_2$. Although it becomes increasingly more difficult to obtain single crystals of $RESn_xSb_2$ of lower Sn content, a single-crystal structure determination of $LaSn_{0.5}Sb_2$ shows that Sn atoms continue to disorder over the same three types of sites in the chains at a reduced partial occupancy of ca. 13% in each but with no particular site preferences [56].

^{119}Sn Mössbauer spectroscopy on the $LaSn_xSb_2$ ($0.1 \leq x \leq 0.7$) series shows that the Sn atoms in the three inequivalent sites have isomer shifts (2.58–2.81 mm s^{-1} relative to SnO_2) close to that of elemental β-Sn (2.52 mm s^{-1}) [56]. This implies that the Sn atoms within these chains are essentially zero-valent. Although it is hard to portray in Fig. 10, on average each Sn atom is bonded to four atoms (two neighbouring Sn and two Sb(2) atoms) and each Sb(2) atom to one Sn atom. Taking a picture in which these Sn–Sn and Sn–Sb bonds are fully covalent, we assign formal charges of Sn^0 and $Sb(2)^{2-}$. With the further assumption that the La–Sn and La–Sb bonds are fully ionic and the atoms in the hypervalent $^2_\infty[Sb]$ square sheet are $Sb(2)^{1-}$, the formulation $(La^{3+})(Sn^0)_x(Sb(1)^{1-})(Sb(2)^{2-})$ suitably accounts for the variable Sn content.

Table 4
Electrical and magnetic properties of $RESn_xSb_2$ [56]

Compound	Properties
$LaSn_{0.7}Sb_2$	Superconducting, $T_C < 2$ K
$CeSn_{0.7}Sb_2$	Metallic with resistivity minimum at ca. 25 K; ferromagnetic, $T_C = 3.5$ K, $M_{sat} = 1.35$ μ_B at 2 K
$CeSn_{0.5}Sb_2$	Ferromagnetic, $T_C = 3.2$ K, $M_{sat} = 1.46$ μ_B at 2 K.
$PrSn_{0.7}Sb_2$	Metallic; no long-range magnetic ordering down to 2 K
$PrSn_{0.5}Sb_2$	No long-range magnetic ordering down to 2 K
$NdSn_{0.7}Sb_2$	Metallic; antiferromagnetic, $T_N = 3.8$ K; metamagnetic, $H_C = 5.5$ T at 2 K
$NdSn_{0.5}Sb_2$	Antiferromagnetic, $T_N = 4.0$ K; metamagnetic, $H_C = 5.4$ T at 2 K
$SmSn_{0.7}Sb_2$	Metallic; no long-range magnetic ordering down to 2 K
$SmSn_{0.5}Sb_2$	No long-range magnetic ordering down to 2 K

The $RESn_xSb_2$ structure can be derived by formally inserting neutral Sn chains into the structure of the parent binary antimonides $RESb_2$, prying the $^2_\infty[RESb_2]$ layers apart. Expanding the structure and increasing the interlayer separations between RE ions as more Sn is inserted will therefore have an effect on electrical and especially magnetic properties, which are summarized in Table 4. All $RESn_{0.7}Sb_2$ compounds are metallic, but with transitions in their resistivity curves [56]. $LaSn_{0.7}Sb_2$ appears to be superconducting below 2 K. $CeSn_{0.7}Sb_2$ and $CeSn_{0.5}Sb_2$ show long-range ferromagnetic interactions with $T_C = 3$–4 K. The lower T_C compared to that in $CeSb_2$ ($T_C = 15$ K) reflects the diminished magnetic interactions in $CeSn_xSb_2$. Field-induced magnetic transitions are observed in the magnetization curves before a saturation magnetization of 1.4 μ_B is reached above 1 T. $PrSn_{0.7}Sb_2$ and $PrSn_{0.5}Sb_2$ do not attain long-range magnetic ordering down to 2 K. $NdSn_{0.7}Sb_2$ and $NdSn_{0.5}Sb_2$ show long-range antiferromagnetic interactions, similar to $NdSb_2$; the ordering temperature T_N decreases accordingly as more Sn is inserted: 8 K for $NdSb_2$, 4.0 K for $NdSn_{0.5}Sb_2$, and 3.8 K for $NdSn_{0.7}Sb_2$. The $NdSn_xSb_2$ compounds also display metamagnetic transitions at $H_C = 5.5$ T at 2 K, and a magnetic phase diagram for $NdSn_{0.7}Sb_2$ has been determined. The long-range antiferromagnetic ordering

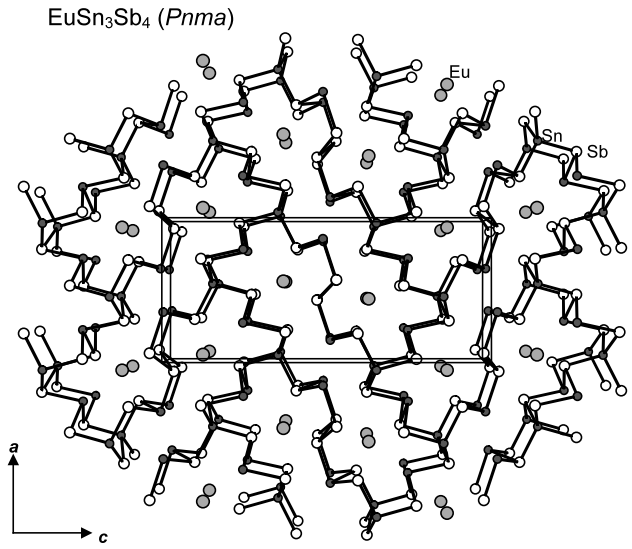

Fig. 11. Structure of $EuSn_3Sb_4$, containing an anionic channel framework built up of 30-membered rings [57].

in $SmSb_2$ disappears on going to $SmSn_{0.7}Sb_2$ and $SmSn_{0.5}Sb_2$, which only show a weak temperature dependence of magnetic susceptibility down to 2 K.

$EuSn_3Sb_4$ [57] is isostructural to $SrSn_3Sb_4$ [58], not surprisingly given the similarity of the ionic radii of Eu^{2+} and Sr^{2+}. It is a classical Zintl compound with an anionic channel structure built up of $SnSb_4$ tetrahedra, $SnSb_3$ trigonal prisms, and Sb–Sb zigzag chains (Fig. 11). Although each atom has a closed-shell configuration and semiconducting properties might have been naïvely expected, additional interactions linking the channels together to form the three-dimensional network induce band broadening of the valence and conduction bands so that the energy gap vanishes. Accordingly, the resistivity curve down to 25 K for $EuSn_3Sb_4$ confirms metallic behaviour [57]. In light of a more recent measurement down to 2 K for the isostructural compound $SrSn_3Sb_4$ suggesting superconductivity at ca. 4 K [59], it would be worthwhile to remeasure the resistivity of $EuSn_3Sb_4$ at lower temperatures.

2.2.6. *RE–Pb–Sb*

La_5Pb_3Sb, an interstitial derivative with the stuffed Mn_5Si_3-type structure discussed earlier [27], and La_4PbSb_2, a solid solution with the *anti*-Th_3P_4-type structure of the parent La_4Sb_3 [53], are the only representatives known in this system. La_4PbSb_2 does not superconduct down to 0.08 K.

2.2.7. *Quaternaries*

The similarity of the layered $REGaSb_2$, $REIn_{0.8}Sb_2$, and $RESn_xSb_2$ structures provides an excellent opportunity to study the effects of size and electron concentration if the different main-group elements M, M′ = Ga, In, and Sn can be mixed to form quaternary phases RE–M–M′–Sb. The series $LaGa_xSn_ySb_2$ can be elaborated [60], but as in the preparation of $LaGaSb_2$, an excess of Ga must be used to avoid formation of $Pr_{12}Ga_4Sb_{23}$-type byproducts. When only a small amount of Sn is added, the Sn atoms simply disorder with Ga atoms in zigzag chains as in the parent $REGaSb_2$ structure: in $LaGa_{0.80(3)}Sn_{0.20}Sb_2$, the zigzag chains now contain a small proportion of Ga–Sn bonds in addition to Ga–Ga bonds. When a large amount of Sn is introduced, the zigzag chains cannot accommodate Sn–Sn bonds which are considerably longer than Ga–Ga bonds, so the Sn atoms reappear in chains of partially occupied sites as in the parent $RESn_{0.75}Sb_2$ structure: in substoichiometric $LaGa_{0.43(3)}Sn_{0.39(3)}Sb_2$, there is disorder between the zigzag chains of Ga sites and linear chains of Sn sites. There is also evidence for the possibility of extensive mixing of In and Sn in the quaternary system $LaIn_xSn_ySb_2$ (ca. $0.1 \leq x, y \leq$ ca. 0.7) [61]. The X-ray powder diffraction patterns of these quaternaries indicate that their structures probably involve random stacking of $^2_\infty[LaSb_2]$ layers with disordered In and Sn chains between them, so that accurate structure determination will no doubt be challenging.

2.3. *Bismuthides*

$Eu_{14}InBi_{11}$, prepared by stoichiometric reaction of the elements in a Ta tube at ca. 1000 °C (with some Eu_4Bi_3 byproduct always being formed) [48], is yet another representative of the $Ca_{14}AlSb_{11}$-type structure; it undergoes an apparently antiferromagnetic transition at 10 K. The *anti*-Th_3P_4-type solid solutions La_4SnBi_2 and $La_4Pb_xBi_{3-x}$ ($0.5 \leq x \leq 1.5$) are known [53], with the latter being superconducting at $T_C = 2.3$–2.5 K. We have evidence for the existence of a ternary La–Ga–Bi phase [62] with a hexagonal structure likely related to that of $La_{13}Ga_8Sb_{21}$. Otherwise, ternary rare-earth main-group bismuthides have not been systematically studied.

3. Structure and bonding

Perhaps the most striking feature in the rare-earth main-group pnictides surveyed is the recurrence of extensive homoatomic bonding of the main-group and pnicogen components. Although it is understandable that the antimonides are the most prone to show hypervalent bonding networks such as Sb square sheets, even a few phosphides and arsenides such as $RESiP_3$ and $RESiAs_3$ display similar pnicogen square sheets. The majority of the ternary antimonides discussed fall into this intermediate category, between 'normal' Zintl phases such as $Yb_5In_2Sb_6$ or $EuSn_3Sb_4$ at one extreme,

where a divalent RE simply substitutes for an alkaline-earth element, and more typical intermetallic phases such as La_4SnSb_2 or La_4PbSb_2 (*anti*-Th_3P_4-type) at the other extreme, where the main-group and pnicogen atoms simply disorder.

To examine the bonding in these complicated structures, we apply a 'retrotheoretical analysis' in which the extended structures are broken up into simpler building blocks of lower dimensionality [63]. The removal of the RE atoms from further consideration, with the assumption that they transfer their electrons to the anionic substructure, simply corresponds to the Zintl concept. What is not so clear, however, is how the ensemble of valence electrons available to the anionic substructure is partitioned.

3.1. Role of RE

Before we examine the anionic substructures, it is worthwhile questioning the assumption of full electron transfer from the RE atoms. The structures of ternary alkali and alkaline-earth main-group pnictides A–M–Pn tend to contain heteroanions with the less electronegative M as the central atom and the more electronegative Pn as bridging ligands that serve to condense together tetrahedral, trigonal pyramidal, or trigonal planar units [12]. In the unusual case of $NaSn_2As_2$ and $SrSn_2As_2$, which are found to adopt the same structure, it is proposed that an incomplete transfer of electrons from Sr to the $[Sn_2As_2]$ substructure entails additional Sn–Sn bonding [12,64]. That is, instead of forming lone pairs, the metalloid atoms satisfy their valence requirements (i.e. octet rule) by forming bonds to themselves. Similarly, the assumption of RE^{3+} ions may be suspect given that many of the structures of the ternary rare-earth main-group antimonides show such extensive homoatomic bonding networks of the metalloid atoms. Band structure calculations on the $La_{13}Ga_8Sb_{21}$ and $RE_{12}Ga_4Sb_{23}$ structures indicate a significant overlap of RE 5d states with the metalloid states [35]. In these calculations, the manifestation of a reduced electron transfer from the RE atoms is evidenced by a shift in the Fermi level compared to a calculation with the RE atoms omitted.

Another clue that shows a link to more typical intermetallic structures is the presence of RE_6 trigonal prisms that share their triangular faces to form columns and are centred by metalloid atoms, as seen in $La_{13}Ga_8Sb_{21}$, $RE_{12}Ga_4Sb_{23}$, Ce_2GeSb_3, and $RE_6Ge_{5-x}Sb_{11+x}$. Such triangular assemblies reflect the tendency of atoms to form close-packed layers in intermetallic structures; they may be regarded as fragments of the WC-type structure in the limit of infinitely large triangular assemblies. Maximizing space-filling cannot be the sole determining principle in these compounds, however. The RE atoms do not attain the very high CNs (12–16) found in typical intermetallics such as the Laves phases [2,3]. Instead, a square antiprism capped by one or two additional atoms is the most common coordination geometry (CN 9 or 10), as shown in Fig. 12. Usually, Sb atoms form the corners of the square antiprism and the other metalloid atoms reside above the square faces (on average, the La atom in $LaSn_{0.75}Sb_2$ is capped by two Sn atoms; Fig. 12d).

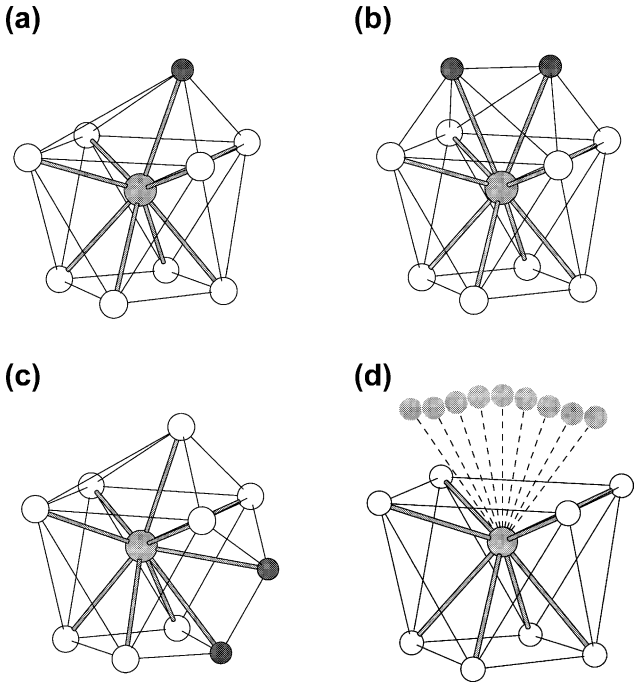

Fig. 12. Common coordination geometries of the RE atom found in ternary rare-earth main-group pnictides. All are based on square antiprisms that are: (a) monocapped (e.g. $LaIn_{0.8}Sb_2$ [40]); (b) bicapped with capping atoms above the same square face (e.g. $REGaSb_2$ [36]); (c) bicapped with capping atoms above different faces (e.g. $RE_6Ge_{5-x}Sb_{11+x}$ [51]); or (d) capped by a chain of partially occupied Sn sites (approximately capped by two atoms, *on average*) in $LaSn_{0.75}Sb_2$ [55,56].

3.2. M–M and Sb–Sb bonding networks

A summary of the major homoatomic bonding patterns seen in the ternary RE–M–Sb compounds is given in Table 5. The metalloid component M generally forms strong 2c–2e$^-$ M–M bonds within pairs or chains. The Ga_6 ring in $La_{13}Ga_8Sb_{21}$ is unusual [34] but another example of it occurs in a La–Ga–Bi compound currently being characterized [62]. Sb shows remarkable versatility in forming classical Sb_2 pairs to weak fractional bonds in nonclassical square sheets and ribbons in these compounds. As a point of reference, a bond distance of 2.908 Å is found for the intralayer contacts and 3.355 Å for the interlayer contacts in elemental Sb [65]. Evaluations of Sb–Sb bond strengths have been presented previously, with the conclusion that, aside from obviously strong single bonds near 2.9

Table 5
Patterns of homoatomic bonds (Å) in rare-earth main-group antimonides RE–M–Sb

Compound	M	Sb	Reference
$La_{13}Ga_8Sb_{21}$	Ga_6 rings, 2.422(5)	Sb_5 ribbons, 3.0934(11)–3.1338(14)	[34]
$Pr_{12}Ga_4Sb_{23}$	Ga_2 pairs, 2.586(4)	Sb_5 ribbons, 3.1088(7)–3.1095(10)	[34]
		Sb_6 ribbons, 3.0085(7)–3.1296(7)	
$SmGaSb_2$	Ga zigzag chains, 2.539(2)	Sb square sheets, 3.0549(2)	[36]
$NdGaSb_2$	Ga zigzag chains, 2.605(3)	Sb square sheets, 3.0749(2)	[36]
$LaIn_{0.8}Sb_2$	In zigzag chains, 2.967(5)	Sb square sheets, 3.119(3)–3.142(3)	[40]
$Yb_5In_2Sb_6$	–	Sb_2 pairs, 2.9437(18)	[41]
Ce_2GeSb_3	–	Sb zigzag chains, 3.111	[49]
$La_6Ge_{2.8(1)}Sb_{13.2(1)}$	M_2 pairs, 2.6154(16)	Sb_3 ribbons, 2.9179(11), (3.3328(11)) [a]	[51]
$Nd_6Ge_{3.6(1)}Sb_{12.4(1)}$	M_2 pairs, 2.5879(14)	Sb_3 ribbons, 2.9175(9), (3.2788(10)) [a]	[51]
$Gd_6Ge_{4.3(1)}Sb_{11.7(1)}$	M_2 pairs, 2.547(2)	Sb_3 ribbons, 3.0780(8) [a]	[51]
$LaSn_{0.75}Sb_2$	Sn chains, 2.814(3)–2.844(3)	Sb square sheets, 3.0952(3)	[55]
$EuSn_3Sb_4$	–	Sb zigzag chains, 2.915(1)	[57]

[a] An Sb_2 zigzag chain is also present in a disordered Ge–Sb puckered sheet. Within such sheets, there are M_2 pairs consisting of a mixture of Ge and Sb atoms.

Å, any contact in the range of 3.0–3.3 Å is potentially a bonding interaction that cannot be neglected [13–15,63]. Square Sb sheets containing this range of Sb–Sb distances are already found in binary rare-earth antimonides such as $YbSb_2$ [66] or $SmSb_2$ [10]. Whether one carries out a rigorous band structure calculation or simply applies the octet rule to each four-bonded Sb atom, the conclusion is that each Sb atom in a square sheet is assigned a count of six electrons: two lone pairs occupy the s and p_z (perpendicular to the sheet) orbitals (or sp_z hybrids thereof, as shown in Scheme 1 below), and the remaining two electrons are distributed over the in-plane p_x and p_y orbitals which overlap with those on neighbouring atoms to form weak Sb–Sb bonds. That is, each Sb atom in a square sheet is assigned an oxidation number of −1, and each Sb–Sb bond is approximately a one-electron bond. The emerging theme in the rare-earth main-group antimonides is the frequent occurrence of Sb ribbons (or 'strips') that are one-dimensional in extent and excised as fragments of a square net [14]. A distinction is made between atoms located in the interior and at the borders of the ribbon. The interior Sb atoms are four-bonded and assigned to be −1, in analogy to the square net, but the border Sb atoms are two-bonded and assigned to be −2 (consistent with three lone pairs and one bonding electron per atom). Although these ribbons were previously seen in the structures of La_6MnSb_{15} [67] and $ZrSb_2$ [68,69], we aver that the variation in widths of these ribbons can be even more extensive, as seen in the rare-earth main-group antimonides (Fig. 13). One can envision that even wider ribbons are possible, and that the examples listed in Table 5 are potentially members of a larger family of compounds. Given that square Pn sheets are also observed in $RESiP_3$ [19–21] and $RESiAs_3$ [22–24], one can anticipate that this theme of pnicogen ribbons should also apply more generally to phosphides and arsenides.

An analysis of the crystal orbital overlap population (COOP) curves for the Sb–Sb contacts in these ribbons or sheets within the actual crystal structures frequently reveals that only weakly antibonding levels are occupied near the Fermi level. Coupled with the broad energy dispersion of the Sb bands, this means that there is relatively little sensitivity of the Sb–Sb bond strengths to small changes in band occupation. As we shall see, this has important consequences.

3.3. Retrotheoretical analysis

To illustrate the basic approach, Fig. 14 shows the analysis of $REGaSb_2$ (which could be adapted for the related layered structures of $LaIn_{0.8}Sb_2$ and $LaSn_xSb_2$) [36]. It is natural to break up the anionic substructure $[GaSb_2]^{3-}$ in $REGaSb_2$ into separate $^2_\infty[GaSb]^{2-}$ and $^2_\infty[Sb]^{1-}$ layers. Assuming a polar Ga–Sb bond, assigning an oxidation state of +1 to Ga (and −3 to Sb) within the $^2_\infty[GaSb]^{2-}$ layer is consistent with the formation of two Ga–Ga bonds to each Ga centre, forming a zigzag chain. The charge on a $^2_\infty[Sb]^{1-}$ square sheet has been rationalized earlier. Band calculations

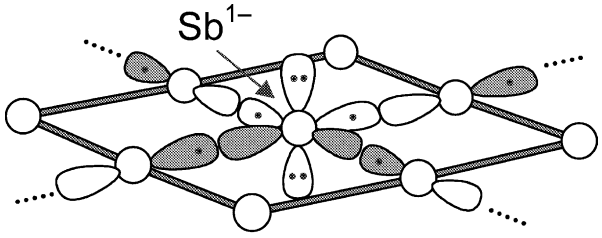

Scheme 1.

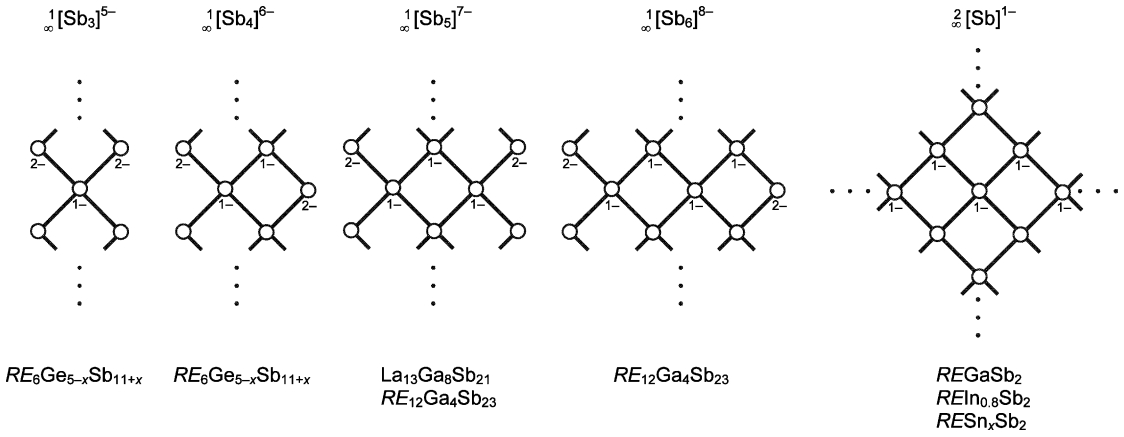

Fig. 13. Planes, chains, and antimonides. The evolution of one-dimensional Sb ribbons of variable width, to the limiting extreme of a two-dimensional square net.

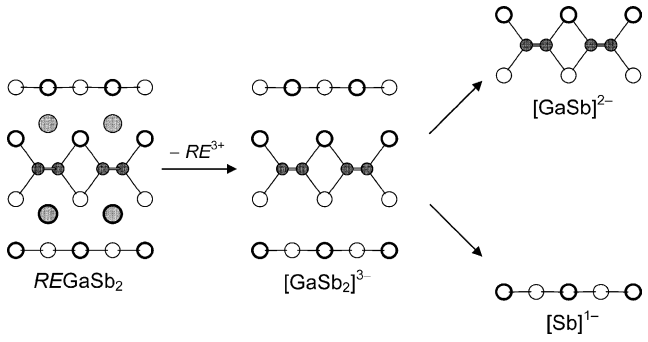

Fig. 14. Retrotheoretical analysis of REGaSb$_2$ [36].

carried out separately for the two layers reveal that the $^2_\infty[GaSb]^{2-}$ layer is a closed-shell system with a band gap between completely filled Ga–Ga and Ga–Sb bonding levels and the empty antibonding levels, whereas the $^2_\infty[Sb]^{1-}$ square sheet gives rise to a continuous distribution of states with essentially nonbonding Sb–Sb character near the Fermi level. When the two layers are reassembled to form the composite structure, a donor–acceptor interaction occurs in which the $^2_\infty[GaSb]^{2-}$ layer gives up some of its electrons to the $^2_\infty[Sb]^{1-}$ square sheet. The Sb square sheet thus acts in its capacity as an electron sink, able to accept additional electrons to an extent that Sb–Sb bonds are weakened only slightly because of the slightly antibonding character of the states being occupied. The argument can be extended to $LaIn_{0.8}Sb_2$, which is found to be substoichiometric in In [40]. Because In is less electronegative than Ga, the states derived from the $^2_\infty[InSb]^{2-}$ layer of a hypothetically stoichiometric $LaInSb_2$ lie higher in energy. The enhanced donor–acceptor interaction entails a greater transfer of electrons to the antibonding Sb–Sb states, to an extent where Sb–Sb bonds would be weakened a little too much. Nature's answer is to introduce vacancies to lower the electron count.

The real utility of retrotheoretical analysis is demonstrated in trying to make sense of the more intricate $RE_{12}Ga_4Sb_{23}$ structure (Fig. 15) [35]. The anionic substructure $[Ga_4Sb_{23}]^{36-}$ can be decomposed into three parts: two isolated $[GaSb_3]$ planar units, an isolated five-atom-wide Sb ribbon, and a $[Ga_2Sb_{12}]$ framework. How the 36 negative charges are to be distributed is unclear. Instead, we analyze each part and assign reasonable charges separately, and then compare the sum of the charges to 36−. The $GaSb_3$ trigonal planar unit is isoelectronic to the familiar boron trihalides; the Ga centre remains formally electron deficient in $[GaSb_3]^{6-}$. The five-atom-wide Sb ribbon is assumed to contain one-electron bonds, and following Fig. 13, it is represented as $[Sb_5]^{7-}$. Breaking Ga–Ga bonds in the $[Ga_2Sb_{12}]$ framework leads to kinked $[GaSb_6]$ sheets that may be regarded as being derived from a square Sb sheet with every seventh diagonal being replaced by a row of Ga atoms. Assumption of one-electron bonds and completion of octets leads to an assignment of $[GaSb_6]^{9-}$. To reform the $[Ga_2Sb_{12}]$ framework, adjacent kinked sheets are stacked so as to direct lone pairs of Ga atoms from adjacent sheets together. To forgo the $2c–4e^-$ repulsion that would otherwise arise, each Ga atom must be oxidized by one electron to give an attractive $2c–2e^-$ interaction, yielding a formulation of $[Ga_2Sb_{12}]^{16-}$. When the charges are tallied up, $[GaSb_3]^{6-}[GaSb_3]^{6-}[Sb_5]^{7-}[Ga_2Sb_{12}]^{16-} = [Ga_4Sb_{23}]^{35-}$, the total charge is one electron less than the 36− expected if the RE atoms had transferred their valence electrons entirely. Again, the most likely candidate for further reduction is the $[Sb_5]$ ribbon. An analysis of COOP curves shows that adding one more electron to bring the charge to 36− is favourable in strengthening the Ga–Ga and Ga–Sb bonds at the expense of only slightly weakening the Sb–Sb bonds within the $[Sb_5]$ ribbons.

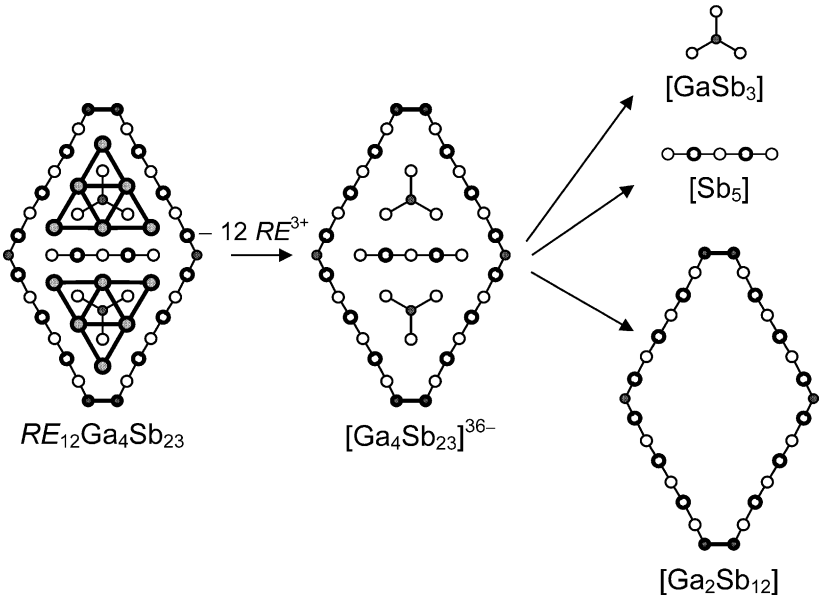

Fig. 15. Retrotheoretical analysis of $RE_{12}Ga_4Sb_{23}$ [35].

4. Conclusion

The rare-earth main-group pnictides adopt structures that show interesting divergences from the corresponding alkali and alkaline-earth systems. Especially for the antimonides, more unusual modes of bonding beyond simple 2c–2e$^-$ heteroatomic interactions appear as the electronegativity differences between metal and metalloid components are reduced. In particular, Sb is notably varied and rich in its homoatomic bonding, forming nonclassical networks such as square nets and ribbons. Although these antimonides show typical characteristics of intermetallic structures, such as the prevalence of metalloid-filled trigonal prisms and high CNs, the electronegativity differences are not so small that the Zintl concept becomes inapplicable. It still serves as a good starting point to help rationalize the bonding in these very complex structures through a fragment or retrotheoretical analysis, if somewhat longer Sb–Sb bonds (3.0–3.3 Å) are counted as approximately one-electron bonds. In cases where the electron counting on the anionic substructure is inconsistent with the assumption of complete transfer of electrons from the RE atoms, the resolution can be traced to the occupation of states near the Fermi level arising from the Sb network. Because of the nonbonding or weakly antibonding nature of these Sb–Sb states, these Sb square nets or ribbons are able to tolerate some degree of oxidation or reduction without undergoing severe distortion.

Perhaps the most exciting direction to which this work is heading involves the characterization of the physical properties. The alkali and alkaline-earth main-group pnictides are predicted to be diamagnetic and semiconducting for the most part, although there can be exceptions. The rare-earth main-group pnictides, however, are likely to display magnetic ordering, owing to the presence of unpaired f electrons from the RE component, and metallic conductivity, especially in the antimonides, arising from broader bands engendered by the Sb networks. To be sure, there remain significant synthetic challenges, but gratifying rewards are in store for the intrepid solid-state chemist.

Acknowledgements

The Natural Sciences and Engineering Research Council of Canada supported this work. Several undergraduate students who have made invaluable contributions to this research receive our gratitude: Ryan W. Hushagen, Joshua A. Eulert, Robert E. Ellenwood, Michael J. Sprague, and Mark G. Morgan.

References

[1] B.G. Hyde, S. Andersson, Inorganic Crystal Structures, Wiley, New York, 1989.
[2] W.B. Pearson, The Crystal Chemistry and Physics of Metals and Alloys, Wiley-Interscience, New York, 1972.
[3] J.H. Westbrook (Ed.), Intermetallic Compounds, Wiley, New York, 1967.
[4] S.M. Kauzlarich (Ed.), Chemistry, Structure, and Bonding of Zintl Phases and Ions, VCH Publishers, New York, 1996.
[5] R. Nesper, Angew. Chem. Int. Ed. Engl. 30 (1991) 789.
[6] H. Schäfer, Annu. Rev. Mater. Sci. 15 (1985) 1.
[7] G.J. Miller, F. Li, H.F. Franzen, J. Am. Chem. Soc. 115 (1993) 3739.
[8] A.K. Ganguli, A.M. Guloy, E.A. Leon-Escamilla, J.D. Corbett, Inorg. Chem. 32 (1993) 4349.

[9] R. Nesper, Prog. Solid State Chem. 20 (1990) 1.
[10] R. Wang, H. Steinfink, Inorg. Chem. 6 (1967) 1685.
[11] J.-T. Zhao, J.D. Corbett, Inorg. Chem. 34 (1995) 378.
[12] B. Eisenmann, G. Cordier, in: S.M. Kauzlarich (Ed.), Chemistry, Structure, and Bonding of Zintl Phases and Ions, VCH Publishers, New York, 1996, pp. 61–137.
[13] G.A. Papoian, R. Hoffmann, Angew. Chem. Int. Ed. 39 (2000) 2408.
[14] G. Papoian, R. Hoffmann, J. Am. Chem. Soc. 123 (2001) 6600.
[15] H. Kleinke, Chem. Soc. Rev. 29 (2000) 411.
[16] H. Kleinke, Chem. Commun. (1998) 2219.
[17] V.I. Torbov, V.I. Chukalin, V.N. Doronin, L.G. Nikolaeva, Z.S. Medvedeva, Russ. J. Inorg. Chem. (Engl. Transl.) 19 (1974) 21.
[18] K.E. Mironov, R.V. Abdullin, Russ. J. Inorg. Chem. (Engl. Transl.) 25 (1980) 1142.
[19] H. Hayakawa, T. Sekine, S. Ono, J. Less-Common Met. 41 (1975) 197.
[20] S. Ono, H. Hayakawa, K. Nomura, Nippon Kagaku Kaishi (1976) 1700.
[21] H. Hayakawa, S. Ono, A. Kobayashi, Y. Sasaki, Nippon Kagaku Kaishi (1978) 1214.
[22] H. Hayakawa, A. Suzuki, S. Ono, J. Less-Common Met. 71 (1980) 235.
[23] H. Hayakawa, A. Suzuki, S. Ono, Nippon Kagaku Kaishi (1984) 697.
[24] H. Hayakawa, S. Ono, J. Less-Common Met. 144 (1988) 177.
[25] F. Hulliger, R. Schmelczer, D. Schwarzenbach, J. Solid State Chem. 21 (1977) 371.
[26] P. Kaiser, W. Jeitschko, J. Solid State Chem. 124 (1996) 346.
[27] A.M. Guloy, J.D. Corbett, Inorg. Chem. 32 (1993) 3532.
[28] A.M. Guloy, J.D. Corbett, J. Solid State Chem. 109 (1994) 352.
[29] M. Somer, W. Carillo-Cabrera, K. Peters, H.G. von Schnering, Z. Kristallogr. 213 (1998) 7.
[30] M. Somer, W. Carillo-Cabrera, K. Peters, H.G. von Schnering, G. Cordier, Z. Kristallogr. 211 (1996) 257.
[31] H.G. von Schnering, M. Hartweg, H. Kalpen, J. Nuss, W. Hönle, Z. Kristallogr. 182 (1988) 238.
[32] J. Nuss, H. Kalpen, W. Hönle, M. Hartweg, H.G. von Schnering, Z. Anorg. Allg. Chem. 623 (1997) 205.
[33] O.S. Zarechnyuk, E.A. Tsygulya, Inorg. Mater. (Engl. Transl.) 2 (1966) 180.
[34] A.M. Mills, A. Mar, Inorg. Chem. 39 (2000) 4599.
[35] A.M. Mills, L. Deakin, A. Mar, Chem. Mater. 13 (2001) 1778.
[36] A.M. Mills, A. Mar, J. Am. Chem. Soc. 123 (2001) 1151.
[37] A.N. Kuliev, G.I. Safaraliev, G.A. Guseinov, Inorg. Mater. (Engl. Transl.) 26 (1990) 422.
[38] A.E. Dwight, Rare Earths Mod. Sci. Technol. 2 (1980) 39.
[39] A. Iandelli, Z. Anorg. Allg. Chem. 330 (1964) 221.
[40] M.J. Ferguson, R.E. Ellenwood, A. Mar, Inorg. Chem. 38 (1999) 4503.
[41] S.-J. Kim, J.R. Ireland, C.R. Kannewurf, M.G. Kanatzidis, J. Solid State Chem. 155 (2000) 55.
[42] P. Verdier, M. Maunaye, R. Marchand, J. Lang, C.R. Séances, Acad. Sci. Sér. C 281 (1975) 457.
[43] P. Verdier, P. L'Haridon, M. Maunaye, Y. Laurent, Acta Crystallogr. Sect. B: Struct. Crystallogr. Cryst. Chem. 32 (1976) 726.
[44] G. Cordier, E. Czech, M. Jakowski, H. Schäfer, Rev. Chim. Minér. 18 (1981) 9.
[45] G. Cordier, H. Schäfer, M. Stelter, Z. Naturforsch. Sect. B: Anorg. Chem. Org. Chem. 40 (1985) 5.
[46] G. Cordier, M. Stelter, Z. Naturforsch. Sect. B: Chem. Sci. 43 (1988) 463.
[47] G. Cordier, H. Schäfer, M. Stelter, Z. Naturforsch. Sect. B: Anorg. Chem. Org. Chem. 39 (1984) 727.
[48] J.Y. Chan, M.E. Wang, A. Rehr, S.M. Kauzlarich, D.J. Webb, Chem. Mater. 9 (1997) 2131.
[49] A.O. Steskiv, V.V. Pavlyuk, O.I. Bodak, Pol. J. Chem. 72 (1998) 956.
[50] A.M. Guloy, J.D. Corbett, Inorg. Chem. 35 (1996) 2616.
[51] R. Lam, R. McDonald, A. Mar, Inorg. Chem. 40 (2001) 952.
[52] L. Deakin, R. Lam, A. Mar, Inorg. Chem. 40 (2001) 960.
[53] F. Hulliger, H.R. Ott, J. Less-Common Met. 55 (1977) 103.
[54] R. Wang, H. Steinfink, A. Raman, Inorg. Chem. 6 (1967) 1298.
[55] M.J. Ferguson, R.W. Hushagen, A. Mar, Inorg. Chem. 35 (1996) 4505.
[56] L. Deakin, M.J. Ferguson, M.J. Sprague, A. Mar, R.D. Sharma, C.H.W. Jones, J. Solid State Chem. 164 (2002) 292.
[57] R. Lam, J. Zhang, A. Mar, J. Solid State Chem. 150 (2000) 371.
[58] D.T. Chow, R. McDonald, A. Mar, Inorg. Chem. 36 (1997) 3750.
[59] L. Deakin, R. Lam, F. Marsiglio, A. Mar, J. Alloys Compd. 338 (2002) 69.
[60] M.G. Morgan, M. Wang, A.M. Mills, A. Mar, manuscript in press.
[61] R.E. Ellenwood, J.A. Eulert, A. Mar, unpublished results.
[62] M.G. Morgan, A. Mar, unpublished results.
[63] G. Papoian, R. Hoffmann, J. Solid State Chem. 139 (1998) 8.
[64] P.C. Schmidt, D. Stahl, B. Eisenmann, R. Kniep, V. Eyert, J. Kübler, J. Solid State Chem. 97 (1992) 93.
[65] J. Donohue, The Structures of the Elements, Wiley, New York, 1974, p. 307.
[66] R. Wang, R. Bodnar, H. Steinfink, Inorg. Chem. 5 (1966) 1468.
[67] O. Sologub, M. Vybornov, P. Rogl, K. Hiebl, G. Cordier, P. Woll, J. Solid State Chem. 122 (1996) 266.
[68] E. Garcia, J.D. Corbett, J. Solid State Chem. 73 (1988) 440.
[69] E. Garcia, J.D. Corbett, J. Solid State Chem. 73 (1988) 452.